DOI: 10.14529/jsfi230103

Saddle Point Method Interpretation of Transient Processes in Car Tires

Kseniia S. Kniazeva[1], ***Yoshinori Saito***[2], ***Andrey I. Korolkov***[1], ***Andrey V. Shanin***[1]

The problem of mechanical excitation of a suspended tire is studied experimentally and theoretically. The tire is considered as an elastic waveguide. Its numerical description is provided by the Waveguide Finite Element Method (WFEM). A case of tire excitation by a δ-shaped pulse is considered, which corresponds to a short kick applied to some point of the tire. The paper focuses on asymptotic analysis of the formal solution. Mainly, a forerunner is evaluated, which is a fast non-stationary wave having an exponential decay. A modification of the saddle point method, namely, a multi-contour saddle point method, is applied for such an estimation. In the framework of this method, we look for the saddle points of the analytical continuation of the dispersion diagram of the waveguide, taking into account that the contours of integration form a family of curves on the dispersion diagram. The tire pulse response is also measured experimentally. A good agreement between the experimentally observed forerunner and its theoretical prediction is shown.

Keywords: transient processes in car tires, forerunner, carcass of the dispersion diagram, complex dispersion diagram, multi-contour saddle point method.

Introduction

Tire road noise is known to be a significant contributor to the environmental noise. Naturally, design of "quiet" tires is of great importance for different tire manufacturers. Investigations on how tire noise is born are held since nearly the middle of the last century. A notable progress is achieved, however there are still some unanswered questions on this topic.

The mechanisms of exterior noise generation by tires are usually divided into aero-acoustic induced and vibration-induced ones [27]. The first type is connected to turbulent air motion mostly, and noise of the second type is produced as a result of interaction of tire vibrations to the surrounding air. In the current paper we describe the generation mechanisms of the second type, namely, we are interested in noise, which can be associated with certain tire eigenmodes.

We consider oscillations in a suspended tire, i. e., a tire not touching the ground. Such a study makes sense since a lot of important processes happen on the part of the tire far from the contact patch.

Since a tire is a resonator, it is natural to represent its motion as a sum of modes:

$$U(t, \varphi, Y) = W_{\nu,j}(Y) e^{-i\omega_{\nu,j} t + i\nu\varphi},$$

where U is the (vector) field of displacements in the tire, φ is the azimuth (or circumferential) angle ($0 \le \varphi \le 2\pi$), $\omega_{\nu,j}$ is an eigenfrequency, j is a mode number, Y is the set of two variables in the transversal cross-section of the tire. Function $W_{\nu,j}(Y)$ is a profile of the mode, its three components describe polarization. Value ν is an integer *circumferential order* of the mode.

There exists a number of papers (for example, [13, 20, 26, 28]) devoted to classification of tire modes. A good classification based on mechanisms of modes behavior could help in control of resonances of a tire. However, it is not a simple task to categorize mode profiles $W_{\nu,j}(Y)$.

[1]Lomonosov Moscow State University, Moscow, Russian Federation
[2]Nihon Michelin Tire Co. Ltd., Ota Site, Ota, Japan

Indeed, for any tire, one can distinguish a number of groups of modes, the profiles of which are similar. For example, there can be identified a class of flexural modes, the cross-section of which bends like a plate, while the circumferential motion is weak. Another class features a strong circumferential motion. Each of these classes is quite numerous. The problem is that a tire also has a lot of mixed modal shapes, which combine properties of different classes. This fact makes the number of modal shapes groups big, such a classification is too complex and arbitrary.

A helpful idea is to introduce a waveguide associated with a given tire [7, 8], which we call a *spiral tire*. To build such a spiral tire, we assume that angle coordinate φ can take real values from $-\infty$ to ∞. Then the circumferential order ν becomes an (angular) wavenumber, and it can take real values rather than integer ones. The modes in the spiral tire have the form

$$W_j(Y;\nu)e^{-i\omega_j(\nu)t+i\nu\varphi}.$$

Possible values of ν and ω form a *real dispersion diagram* with continuous modal branches $\omega_j(\nu)$. Modes of the initial non-spiral tire can be obtained from the spiral tire dispersion diagram by picking out the modes with integer ν. Indeed, a tire in this formulation is a segment of a waveguide, $0 \le \varphi \le 2\pi$, on the ends of which the periodicity conditions are imposed.

The modes of the spiral tire with similar modal shapes form branches of the dispersion diagram. The mixed modal shapes appear, where these branches come closer to each other. Usually, such behavior of the modal branches is referred to as *avoided crossing* [15], *avoiding crossing* [22], *mode repulsion* [14], *veering* [26], *diabolical points* [1], *mode splitting, double cusps, osculation points* [10], etc.

The most important reason for building the dispersion diagram of a "spiral tire" (or of any other waveguide) is that it enables to predict the propagation speed for narrow-band modal pulses. This concept is known as *group velocity*, and it can be considered as the speed of energy transfer in a waveguide [25]. The group velocity reasoning is based on the stationary phase method. Namely, for given large φ and t, the point on the dispersion diagram with

$$\frac{d\omega}{d\nu} = \frac{\varphi}{t} \tag{1}$$

is a stationary phase point for the corresponding Fourier integral, and the field is estimated by a local integration near this point. Thus, $d\omega/d\nu$ can be treated as an angular group velocity. The linear group velocity is

$$v_{gr} = r\frac{d\omega}{d\nu}, \tag{2}$$

where r is the radius of the tire. In the standard analysis, this reasoning is held only on a real dispersion diagram. The resulting field components may have some decay due to dispersion, but the amplitude behaves like a power of propagation distance φ (not exponentially).

A research held by Bolton et al. [3] showed that waveguide propagation in tires can be observed experimentally. The authors excited a tire by a random force and measured velocity on a tire surface at different points by a laser vibrometer. After the data had been processed, the pulse response was obtained. Authors observed exponentially decaying waves, i. e., with ν and ω having non-zero imaginary parts. Applying Fourier transform, the authors identified $\mathrm{Re}[\nu]$ and $\mathrm{Re}[\omega]$ for the most effectively excited modes. To calculate $\mathrm{Im}[\nu]$, the authors applied the Prony series method. The results showed that excited waves were formed by some spots of the *complex dispersion diagram* (see below) of a "spiral tire". Another result of the study was the identification of the modal shapes of the excited modes. They are flexural modes with different

transversal index j and a fast mode connected with extension of the tread and having strong displacement in the circumferential displacement.

It was shown in [18, 19], and later on in [21, 22, 24] that the dispersion diagram for a waveguide can be analytically continued into the domain of complex values of ν and ω to obtain the *complex dispersion diagram*. In other words, the complex dispersion diagram is a set of all, complex and real, solutions of the dispersion equation. Studying of the complex dispersion diagram instead of the real one can help one to describe exponentially decaying transient processes in a waveguide. Indeed, instead of the stationary phase method one should use the saddle point method (which is essentially the same).

In the current paper, we develop a method to estimate a response on a δ-shaped force applied to some point on a suspended tire. Our method allows one to predict pulses in a tire and find modal shapes corresponding to these pulses. We are especially interested in *forerunners*, the propagation velocity of which is higher than any group velocity on the real dispersion diagram. Such pulses are of interest in the context of tire noise because they can effectively radiate sound into the surrounding air [3, 27]. The forerunners typically possess exponential decay, but this decay is not strong enough to make the amplitude negligibly small.

Note that the forerunners are a diffraction phenomenon and their attenuation is not connected to damping in tire compounds materials. In this paper we consider only the tires made of materials without energy losses. Indeed, this is a slightly idealized formulation. Beside the simplifications mentioned above, we ignore the interaction of elastic modes with the cavity modes and the radiation of sound into the outer air.

In this paper we describe the wave process in the tire by a WFEM equation (3) (see below) and apply to it a technique similar to the one described in [24], i. e., we find the solution in the form of a Fourier transform and estimate the integrals by the saddle point method assuming that φ is large enough. As it is known from the standard theory, the saddle point method starts with finding of the saddle (or stationary) points on the dispersion diagram, i. e., the points for which the equation (1) is valid for a given value φ/t. Then, one should deform the contours of integration in the initial integrals in such a way that they pass through some of the saddle points and the integrand decays exponentially outside the saddle points. Finally, one should estimate the integral near the saddle points.

Each saddle point on the complex dispersion diagram is related to three values: ν, ω, and the ratio φ/t. A set of all complex saddle points for all admissible (i. e., real) values of φ/t is called *a carcass* of the dispersion diagram. The real dispersion diagram belongs to the carcass as a whole, but there are also important complex branches of the carcass that describe decaying pulses. The latter can give significant contribution into the wave field for moderately large values of φ.

Thus, to estimate the wave field, we make the following steps:

- study the complex dispersion diagram for a tire;
- search for carcass points in the complex domain of ν and ω;
- estimate their contribution into the field;
- sum up contributions from different carcass points.

The plan of the paper is as follows. Some details of the experimental data are described in Section 1. In Section 2 a WFEM equation is formulated. In Section 3 we find a solution in the form of double integral over ν and ω. Then, applying the residue method, we find modal decomposition for the pulse response of a spiral tire. Also, a complex dispersion diagram is discussed. The

carcass for a tire is built in Section 4. The procedure of estimation of the contributions of the carcass points is described in Section 5. In Section 6 we compare the experimental results and the theoretical predictions of the fast transient waves field. Then we make a conclusion.

1. Experimental Evidence of Forerunners in a Tire

Here we describe an experiment for measurement of the pulse response in a suspended tire. The geometry of the experiment is shown in Fig. 1 and Fig. 2. A tire is excited by a force applied to some point on the outer surface of the tire located at the sagittal (central) plane. The force is directed radially towards the tire center. Let the azimuth coordinate of the source be equal to 0°. The time profile of the force is a δ-function[3]. A detector is placed also in the sagittal plane in different positions characterized by the azimuth angle φ. The detector is one-axis, polarized normally to the tire. The detector provides the oscillation acceleration a_n of a point of the tire.

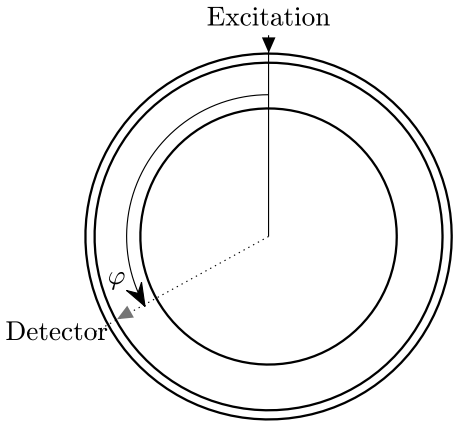

Figure 1. Side view of a tire

The front parts of three typical profiles of pulse response are shown in Fig. 3. From this data, one can easily find that velocity of propagation of the maxima in the area $t < 4$ s is about 350 m/s, and velocity of propagation of maxima in the right part of the figure is about 70 m/s. Let us compare these values to the values of the group velocities on the real dispersion diagram.

A real dispersion diagram for the considered spiral tire is shown in Fig. 4. Corresponding group velocities are plot in Fig. 5. One can see that the maximum value of the group velocity is about 250 m/s. Pulses propagating with velocities higher than this value are the forerunners, in particular, the first pulse in Fig. 3 is a forerunner. The slow pulse appears to be described by the real dispersion diagram, and it corresponds mainly to flexural modes.

Due to the way of the excitation and the fact that the considered tire was almost symmetrical with respect to the central plane, the most effectively excited modes must have significant radial displacement in the central part of a cross-section. One can check that points satisfying this characteristic are located below the line $v_{gr} = 142$ m/s, this area is shown by grey in Fig. 5. That is, we can expect that the wave field for $142 < r\varphi/t < 250$ (m/s) is also formed by some pulses, whose nature is close to the forerunners.

[3]Indeed, such time profile is a result of a correlation-based data processing. We omit details here.

(a) Source position 0° (b) Detector position φ

Figure 2. Tire profiles at the source and the detector azimuth positions

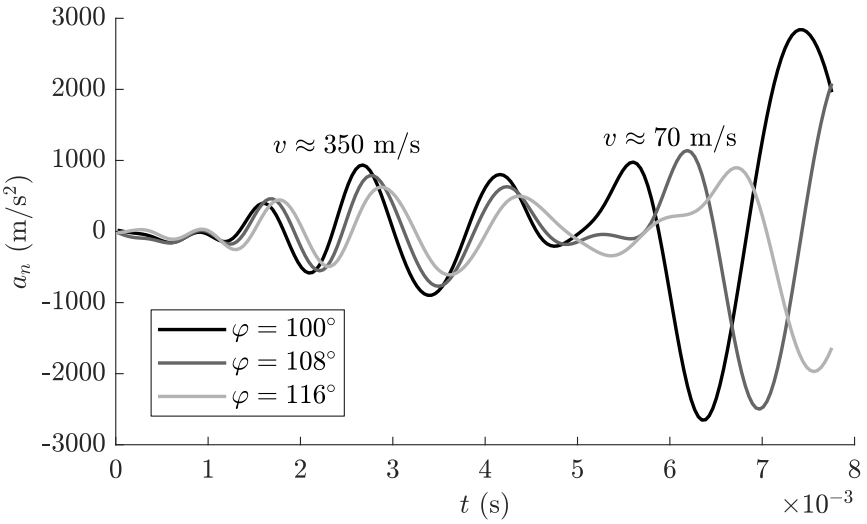

Figure 3. Pulse response of a tire

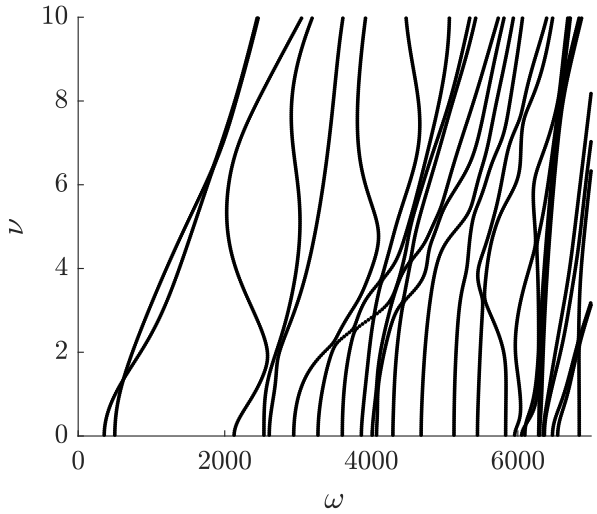

Figure 4. Real dispersion diagram for the chosen tire

We should note that the critical velocity of the pulse in noise-related application is the velocity of sound in air, that is 343 m/s under normal conditions. An elastic pulse that travels faster can radiate a powerful airborne noise due to Cherenkov's mechanism. Indeed, formally, this should be the *phase* velocity of the pulse, i. e., the velocity of pulse maxima/minima. However, as we see below, in our case the phase and group velocities are close to each other.

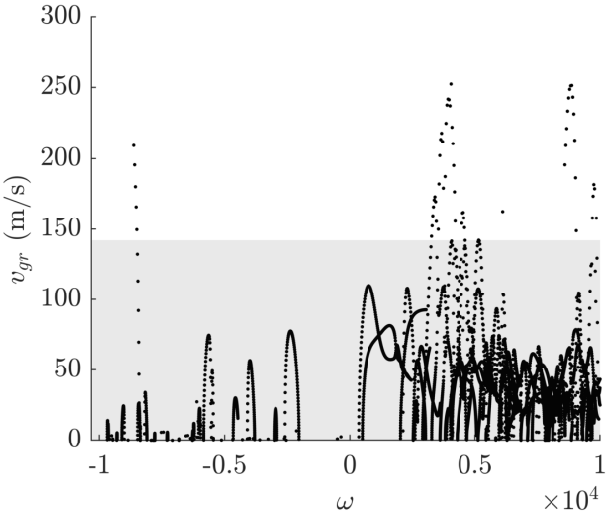

Figure 5. Group velocities for real ω for the chosen tire. Stationary points significantly contributing to the field (due to the excitation way) are located in the grey area

2. Numerical Description of the Tire Using WFEM

We assume that the tire is homogeneous in the angular direction and that the tire cross-section is described by a dense enough mesh. The field is described by values of three spatial components of displacement in each of the mesh nodes. These values form a vector of unknowns $\mathrm{U}(t;\varphi)$. The dimension of this vector is $3N$, where N is the number of mesh nodes on the cross-section of the tire. It is shown in [7, 8, 11, 16] that a good mathematical model for such a tire is *Waveguide Finite Element Method* (WFEM). The method is also called *Semi-analytical finite element* method [14], *Hybrid two-dimensional finite element* method [11], *Matrix Klein-Gordon equation (MKGE)* [12]. In the framework of this method, the field is described by a partial differential equation for U:

$$\left(\mathbf{D}_2\partial_\varphi^2 + \mathbf{D}_1\partial_\varphi + \mathbf{D}_0 - \mathbf{M}\partial_t^2\right)\mathrm{U}(t,\varphi) = \mathrm{F}(t,\varphi), \qquad -\infty < \varphi, t < \infty. \tag{3}$$

The right-hand side $\mathrm{F}(t,\varphi)$ is a vector that describes the excitation. Matrices $\mathbf{D}_2, \mathbf{D}_1, \mathbf{D}_0, \mathbf{M}$ are constant; they depend on the tire structure and materials. Since we ignore the attenuation in the materials forming the tire, matrices $\mathbf{D}_2, \mathbf{D}_1, \mathbf{D}_0, \mathbf{M}$ are assumed to be real and having the following properties:

$$\mathbf{M}^T = \mathbf{M}, \quad \mathbf{D}_0^T = \mathbf{D}_0, \quad \mathbf{D}_1^T = -\mathbf{D}_1, \quad \mathbf{D}_2^T = \mathbf{D}_2. \tag{4}$$

Besides, matrices $\mathbf{M}$ and $\mathbf{D}_2$ should be positive-definite, and $\mathbf{D}_0$ should be a non-negative definite matrix. The matrices $\mathbf{D}_m$ and $\mathbf{M}$ are provided by mechanical modeling (say, FEM-based) and contain the whole mechanical structure of the tire. Below we do not consider this mechanical matter and concentrate on the mathematical properties of (3). A brief derivation of WFEM (3) is described in [23].

According to the experimental set-up, we assume that the excitation is delta-shaped with respect to t and φ:

$$\mathrm{F}\delta(t)\delta(\varphi),$$

where F is a constant vector. Since the force is applied to a small spot on the tire surface and has a radial polarization, we assume that F has a single non-zero component corresponding to a node of application and a polarization of the force.

3. Formal Solution of the Governing Equation

Let us find a formal solution of (3). Let us apply the Fourier transform with respect to φ and Laplace transform with respect to t. The result is a linear algebraic system:

$$\mathbf{P}\widetilde{\mathrm{U}} = \mathrm{F}, \tag{5}$$

where $\widetilde{\mathrm{U}} = \widetilde{\mathrm{U}}(\omega, \nu)$ is a Fourier-Laplace image of $\mathrm{U}(t, \varphi)$, $\mathbf{P}$ is a matrix defined as

$$\mathbf{P} = \mathbf{P}(\omega, \nu) \equiv \omega^2\mathbf{M} - \nu^2\mathbf{D}_2 + i\nu\mathbf{D}_1 + \mathbf{D}_0. \tag{6}$$

Matrix equation (5) can be solved provided $\mathbf{P}$ is non-singular. By inverting the Fourier and Laplace transforms, let us obtain a solution in a double integral form:

$$\mathrm{U}(t, \varphi) = \frac{1}{4\pi^2} \int\limits_{-\infty}^{\infty} \int\limits_{-\infty+i\epsilon}^{\infty+i\epsilon} \mathbf{P}^{-1}\mathrm{F}e^{i\nu\varphi - i\omega t}\, d\omega\, d\nu, \tag{7}$$

where ϵ is an arbitrary small positive value (it comes from the Mellin's transform and enforces the causality of (7)).

Let us fix some value ν and consider the inner integral. According to the Jordan's lemma one can close the integral in the lower half of the complex ω-plane. Applying the residue method, one can obtain the series-integral representation:

$$\mathrm{U}(t, \varphi) = -\frac{i}{2\pi} \sum_j \int\limits_{-\infty}^{\infty} \mathrm{Res}[\mathbf{P}^{-1}\mathrm{F}e^{i\nu\varphi - i\omega t}, \omega_j(\nu)]\, d\nu, \tag{8}$$

where $\omega_j(\nu)$ are solutions of the dispersion equation

$$\det \mathbf{P}(\omega, \nu) = 0 \tag{9}$$

with respect to ω that lie inside the enclosed integral contour on the ω-plane. According to the reality statement [7] all poles of the integrand of the integral in (7) belong to the real ω-axis, and, consequently, all of them participate in (8).

One can derive (see, for example, [16]) that

$$\mathrm{Res}[\mathbf{P}^{-1}, \omega_j(\nu)] = \frac{\mathrm{W}_j\mathrm{V}_j}{2\omega_j(\nu)\mathrm{V}_j\mathbf{M}\mathrm{W}_j}, \tag{10}$$

where $\mathrm{W}_j = \mathrm{W}(\nu, \omega_j(\nu))$ and $\mathrm{V}_j = \mathrm{V}(\nu, \omega_j(\nu))$ are eigenvectors of the left and right eigenvalue problems:

$$\mathbf{P}\mathrm{W} = 0, \qquad \mathrm{V}\mathbf{P} = 0. \tag{11}$$

Hence,

$$\mathrm{U}(t, \varphi) = -\frac{i}{4\pi} \sum_j \int\limits_{-\infty}^{\infty} \frac{\mathrm{W}_j\mathrm{V}_j\mathrm{F}}{\omega_j(\nu)\mathrm{V}_j\mathbf{M}\mathrm{W}_j} e^{i\nu\varphi - i\omega_j(\nu)t}\, d\nu. \tag{12}$$

The dispersion equation (9) can be considered as an equation for ω with a parameter ν. The equation has generally $6N$ solutions $\omega_j(\nu)$ ($3N$ is the dimension of U). It has been shown in [18, 19, 21, 22] that solutions $\omega_j(\nu)$ can be analytically continued into the complex domain of ν to form a Riemann surface R of a multi-valued function $\omega(\nu)$, which is defined implicitly by (9). The index j over which the summation (12) is performed corresponds to number of a sheets of R. Taking this into consideration, one can rewrite (12) as follows:

$$\mathrm{U}(t,\varphi) = -\frac{i}{4\pi} \int\limits_{\sum_j \gamma_j} \frac{\mathrm{WVF}}{\omega(\nu)\mathrm{V}\mathbf{M}\mathrm{W}} e^{i\nu\varphi - i\omega(\nu)t}\, d\nu, \tag{13}$$

where γ_j are all preimages of the positively oriented real axis ν on the Riemann surface R, $\mathrm{W} = \mathrm{W}(\nu, \omega(\nu))$, $\mathrm{V} = \mathrm{V}(\nu, \omega(\nu))$.

The obtained solution (13) is valid for any waveguide. Its problem is that it does not give a clear understanding of the field structure and of wave pulses propagating in the waveguide. To obtain an insight into the transient processes, we apply a *multi-contour saddle point method* [24]. Unlike the usual saddle point method, to estimate (13), we need to perform the integration on the Riemann surface R having a complicated set of branch points. Thus, before applying the multi-contour saddle point method we need to study the structure of R.

In [23, 24] we demonstrated that it is relevant to consider the Riemann surface R as a projection of a manifold H onto the ν-plane. The manifold H is a set of all possible complex solutions (ω, ν) of the dispersion equation, we call it a *complex dispersion diagram*. Note that since points of H are restricted by one equation (9), the manifold H has complex dimension 1, which is real dimension 2.

Instead of projecting of H onto ν-plane, one can project it onto ω-plane. The result is the Riemann surface R' of a multivalued function $\nu(\omega)$, the sheets of which are solutions of (9) with ω taken as a parameter. Such projections result in branch points on the Riemann surfaces, which should be taken into account while deforming the integration contours. Compared to R and R', manifold H is smooth, since it is defined by a polynomial equation (9). Thus, the contours of integration can be *freely* deformed on H.

Another consequence of the smoothness of H is that the corresponding modal shapes (eigenvectors) change smoothly when the point (ω, ν) is moving along a continuous curve on H. This fact explains the interchange of the modal shapes near avoiding crossings of the real dispersion diagram.

Also, we can make an obvious conjecture that manifold H is not connected, if, physically, the waveguide can be split into isolated subsystems.

Let us make a short note on numerical solution of the dispersion equation (9). Indeed, this is a polynomial equation of a high dimension. We prefer to consider this equation as a generalized eigenvalue problem, in which ω^2 is the eigenvalue and ν is a complex parameter. Modern systems of linear algebra solve such problems very efficiently, namely, they are capable of finding, say, about 50 smallest or largest eigenvalues. This fits our needs. All complex and real dispersion diagrams below are built this way. As a by-product of this procedure, we obtain right or left eigenvectors, i. e., solutions of (11).

We are going to use a formula for the angular group velocity [2, 7, 14, 16]:

$$\Omega_{gr} \equiv \frac{d\omega}{d\nu} = \frac{2\nu\mathrm{V}\mathbf{D}_2\mathrm{W} - i\mathrm{V}\mathbf{D}_1\mathrm{W}}{2\omega\mathrm{V}\mathbf{M}\mathrm{W}}. \tag{14}$$

The formula can be easily derived from (11). This formula allows us to avoid numerical differentiation of the function $\omega(\nu)$.

4. Carcass of the Dispersion Diagram

The main goal of the current paper is to estimate asymptotically the expression (13) and indicate the parts of the complex dispersion diagram mainly contributing into the field by the multi-contour saddle point method.

The equation (13) can be rewritten:

$$\mathrm{U}(t,\varphi) = -\frac{i}{4\pi}\int_{\sum_j \gamma_j} \frac{\mathrm{WVF}}{\omega(\nu)\mathrm{V}\mathbf{M}\mathrm{W}} e^{i\varphi g(\nu,\omega)}\, d\nu, \tag{15}$$

where $g(\omega,\nu)$ is a *phase function*

$$g(\omega,\nu) = \nu - \omega/\Omega, \tag{16}$$

Ω is a *formal angular velocity*

$$\Omega \equiv \varphi/t. \tag{17}$$

According to the saddle point method, asymptotic estimation of an integral is a sum of saddle point integrals, and the saddle points are the points where derivative of the phase function is zero:

$$\frac{dg(\omega,\nu)}{d\nu} = 0, \qquad p = (\omega,\nu) \in H. \tag{18}$$

Substituting (16), one can obtain (1). Note that we assume that

$$\left.\frac{d^2 g(\omega,\nu)}{d\nu^2}\right|_p \neq 0$$

at each saddle point. If this is not true, a more elaborate asymptotic (e.g., an Airy one) is needed to be built.

Using function (16), we obtain the condition for finding the saddle point

$$\Omega_{gr}(p) = \Omega, \tag{19}$$

where the function $\Omega_{gr}(p)$ is defined by (14).

Let us consider all points $p \in H$, real and complex, and find the set of all such points that $\Omega(p)$ is real. Indeed, potentially any such point may become a saddle point for some Ω. This set is called a *carcass of the dispersion diagram*.

Not all points of the carcass contribute into the field. Namely, to estimate the integral (13) for certain (t,φ), one should deform the initial integration contour into the steepest descend contour. The latter will pass through some points obeying the relation (19) (and thus contribute to the field), but not necessarily through each of them. The points $p \in H$, through which the steepest descend contour passes when $\varphi/t = \Omega_{gr}(p)$, are called *active* points of carcass, and the rest ones are *not active*.

Obviously, points of the real dispersion diagram satisfy (1), i. e., belong to carcass. Moreover, these points are active, because they define far field, according to the stationary phase method.

A good example of active and not active saddle points is provided by an example based on the integral representation of the Airy function:

$$\mathrm{Ai}(\xi) = \frac{\sqrt{\xi}}{2\pi} \int \exp\{i\xi^{3/2}(\tau^3/3 + \tau)\} d\tau.$$

For large positive ξ, there are two saddle points, $\tau = \pm i$, but only the point $\tau = i$ is active, since the contour of integration should be shifted into the upper half-plane.

The procedure of deformation of the initial contour of integration into a steepest descend one is quite complicated. Fortunately, there exists an efficient algorithm of finding the active points on the carcass without making the whole deformation [6, 24]. The algorithm is as follows:

1. We consider only $\varphi, t > 0$, so carcass points with $\Omega_{gr} < 0$ are marked as not active.
2. Carcass points p with $\mathrm{Im}[g(p)] < 0$ are marked as not active.
3. From other carcass points two contours of steepest descend of $\mathrm{Im}[g]$ are built. If
   - both of them hit the real axis ν, then the point is not active;
   - both of the contours go to infinity on the complex plane ν, then the point is also not active;
   - only one of the contours hits the real axis, then the point is active.

The results of building a carcass and finding active points on the carcass are shown in Fig. 6. As one can see the carcass is composed of 1D curves (branches). We assume that each branch corresponds to a certain mode shape (at least that the mode shape varies continuously along the branch). Thus, one can associate a mode with each branch (corresponding pulses are attenuating).

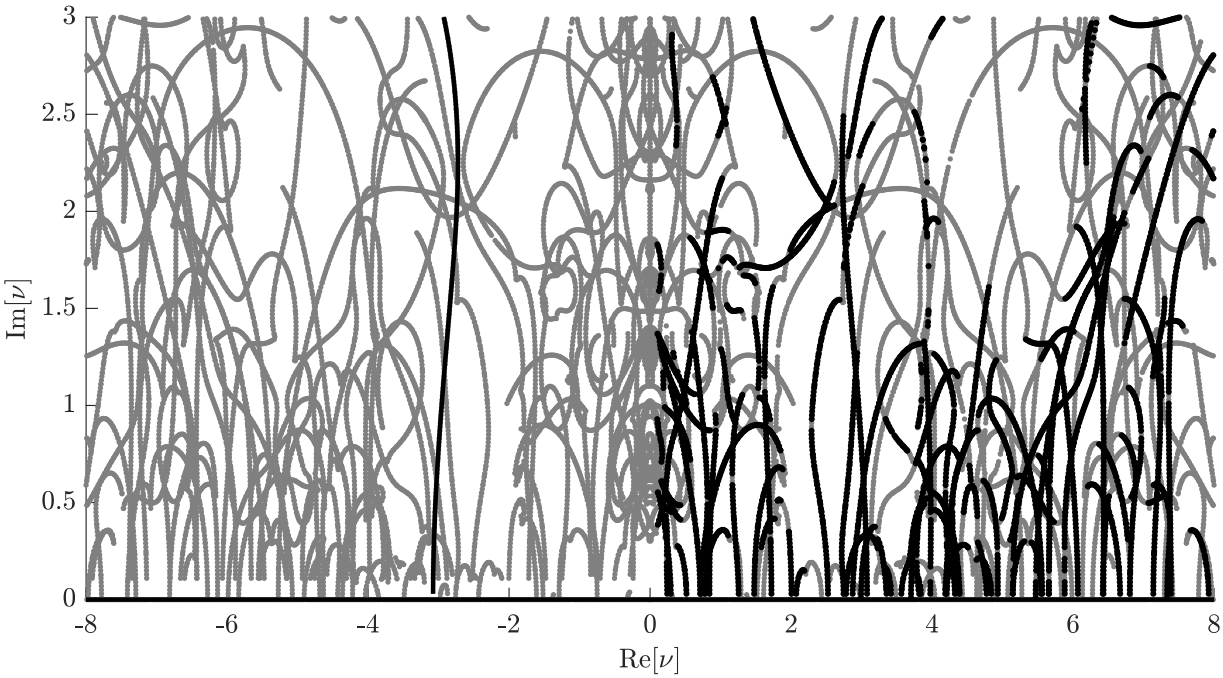

Figure 6. Projection of the carcass on ν-plane: found not active points (grey), active branches (black)

Most of the active carcass branches start from the real axis. The points, where the complex carcass branches start to grow from the real axis, are the points of the group velocity extremes (maxima or minima). As it is known [17] such points provide Airy-type asymptotics.

There can exist points with negative group velocities on the real dispersion diagram (it can be seen in the real dispersion diagram Fig. 4). It follows from the dispersion equation (9) that if a point with positive real ν and ω has a negative group velocity, then the point $(-\nu, \omega)$ has the opposite (positive) value of the group velocity. Such points can also become start points for some complex carcass branches. One of such active carcass branches can be found in the domain $\mathrm{Re}[\nu] < 0$ in Fig. 6.

5. Computing Field Asymptotics at Active Saddle Points

According to the saddle point method, (13) can be represented as a sum of saddle point integrals:

$$\mathrm{U}(t, \varphi) \approx \sum_m \mathrm{U}_{*m}(t, \varphi), \tag{20}$$

where $\mathrm{U}_{*m}(t, \varphi)$ is a contribution of the m-th active carcass point.

Since each active carcass branch is a curve on which Ω changes monotonically, a carcass branch forms a pulse. Our plan is to calculate the field for each of the active carcass branches and then sum them up.

Formula for a contribution U_{*m} of a carcass point (ω_{*m}, ν_{*m}) into the full wave field can be derived in a rather standard way (see, for example, [4]):

$$\mathrm{U}_{*m} = \pm i \sqrt{\frac{1}{2\pi t \left| \frac{d^2\omega}{d\nu^2}\Big|_{\nu_{*m}} \right|}} \exp\left\{ -i \left(\frac{1}{2} \arg\left(\frac{d^2\omega}{d\nu^2}\Big|_{\nu_{*m}} \right) + \pi/4 \right) \right\} \frac{\mathrm{W}_{*m} \mathrm{V}_{*m} \mathrm{F}\, e^{i\nu_{*m}\varphi - i\omega_{*m} t}}{2\omega_{*m} \mathrm{V}_{*m} \mathbf{M} \mathrm{W}_{*m}}, \tag{21}$$

where $\mathrm{W}_{*m} = \mathrm{W}(\omega_{*m}, \nu_{*m})$ and $\mathrm{V}_{*m} = \mathrm{V}_{*m}(\omega_{*m}, \nu_{*m})$ are the (right/left) eigenvectors at the carcass point. The sign in (21) is chosen as follows:

- "minus" if
$$\frac{\pi}{2} < \arg\left(\frac{d^2\omega}{d\nu^2}\Big|_{\nu_{*m}} \right) \le \pi,$$
- "plus" if
$$-\pi < \arg\left(\frac{d^2\omega}{d\nu^2}\Big|_{\nu_{*m}} \right) < \frac{\pi}{2}.$$

Let us recall that the detector measures the radial acceleration a_n in the inner central point of the tire cross-section φ (see Fig. 2). Similar to (20), value a_n can be represented as a sum of the saddle point contributions:

$$a_n(t) \approx \sum_m (a_n)_{*m}(t). \tag{22}$$

Each of the acceleration contributions $(a_n)_{*m}$ is the second time derivative of the corresponding saddle point contribution into the displacement field $(u_n)_{*m}$:

$$(a_n)_{*m}(t) = -\omega_{*m}^2 (u_n)_{*m}(t). \tag{23}$$

A displacement contribution $(u_n)_{*m}$ is the necessary component of the vector U_{*m} calculated by (21).

In Fig. 7 we plot examples of the pulses formed by some of the active carcass branches. The detector position was $\varphi = 100°$. The legend of the figures shows the point on the real ν-axis,

where the active carcass branches start to grow into the complex domain. For example, the most left black branch in Fig. 6 intersects the real axis at $\nu \approx -3.08$. According to the legend for Fig. 7b), this value corresponds to the black dashed line.

One can see that most of the pulses are oscillating and attenuating for small t. Another observation is that there is no prevailing pulse, which determines the field for small t. Instead, there are few dozens of pulses, the amplitude of which are of the same order.

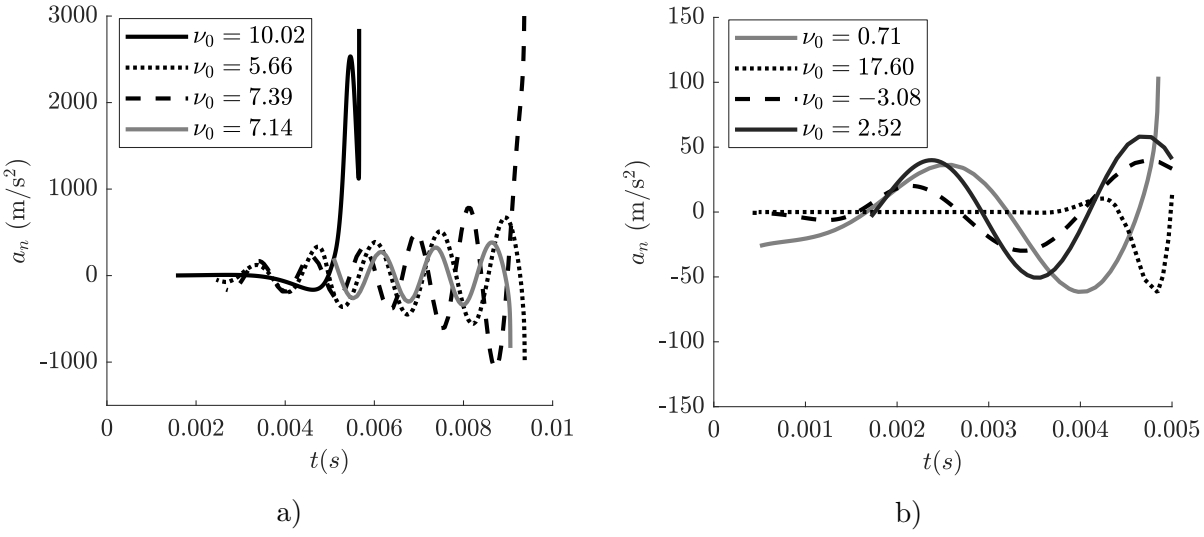

Figure 7. Examples of pulses formed by some of the found active carcass branches. The detector is placed at $\varphi = 100°$

6. Comparison of the Experimental and Theoretical Results

Finally, we find the sum of the calculated pulses for the tire and compare it to the experimental results (see Fig. 8). The black curves in the figure show the saddle point asymptotic, the grey ones show the experiment data.

The area, where the stationary points of the real dispersion diagram can contribute to the field, is highlighted by light grey. As it was discussed in Section 1, the boundary of this area is defined by the maximum group velocity on the real dispersion diagram corresponding to a modal shape with strong radial displacement in the center of a tire cross-section. Since we have considered only the complex branches of the carcass, the curves are not supposed to coincide in the grey area.

We observe that *before* the light grey domain our method describes the wave field adequately. We obtain that the forerunners field is formed by approximately 20 complex carcass branches.

It is worth to recall also that we excluded dissipation losses from our model. Probably, if there were a good instrument to describe the attenuation correctly, even better results could be obtained. However, the problem of description of energy losses in tires is known to be difficult. In a suspended tire the attenuation occurs, mainly, due to the hysteretic character of rubber deformation (see, for example, [5, 9]).

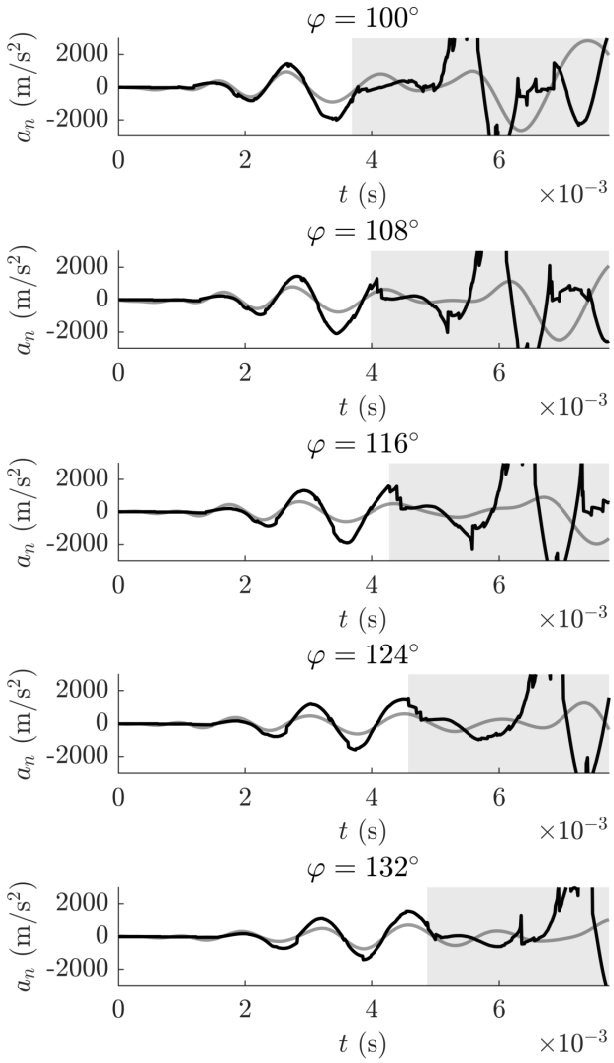

Figure 8. δ-pulse response of the tire for different detector positions: experimental results (grey curves) and the saddle point asymptotics (black curves). Light grey area is the area, where the stationary points of the real dispersion diagram start to contribute

Conclusion

In the current paper, we study non-stationary forerunners in a mechanically excited suspended tire. The consideration is held experimentally and theoretically.

The theoretical model of the tire is provided by a WFEM equation (3). A formal solution is obtained in the form of a sum of integrals (12). We apply the multi-contour saddle point method to evaluate the field contribution corresponding to forerunners.

In the framework of the method, firstly, we compute the complex dispersion diagram of the tire by numerical solution of the eigenproblem (11). After that, we find a carcass, i. e., a set of points on the complex dispersion diagram, on which the value of $d\omega/d\nu$ is real. Then, we classify the found carcass points into active and not active ones by means of the algorithm developed in [6, 24]. The active carcass points are shown to form branches, each of which corresponds to a certain pulse. Finally, to obtain an asymptotic estimation of the non-stationary field, we sum all the calculated pulses.

An asymptotic estimation of a pulse response for a tire is calculated by this method. Then it is compared to the tire pulse response obtained by the experiment briefly discussed in the paper.

A good agreement is observed between the theoretically predicted shape of the forerunners and the experimentaly measured pulses.

An important and slightly unexpected conclusion is that the forerunner is described well only by a considerable number of carcass branches (about 20). This probably means that the forerunner is a *ray pulse* rather than a *modal pulse*. Still, we are not aware of a convenient theory of rays in systems described by WFEM equation. Our finding may be a good motivation for building of such a theory.

References

1. Berry, M.V., Wilkinson, M.: Diabolical points in the spectra of triangles. Proceedings of the Royal Society of London. A. Mathematical and Physical Sciences 392(1802), 15–43 (mar 1984). https://doi.org/10.1098/rspa.1984.0022
2. Biot, M.A.: General theorems on the equivalence of group velocity and energy transport. Physical Review 105(4), 1129–1137 (feb 1957). https://doi.org/10.1103/physrev.105.1129
3. Bolton, J.S., Kim, Y.J.: Wave number domain representation of tire vibration. In: Proceedings of Inter-noise 2000. vol. 1, pp. 184–190 (2000)
4. Borovikov, V.A.: Uniform stationary phase method. IEEE (1994)
5. Collins, J.M., Jackson, W.L., Oubridge, P.S.: Relevance of elastic and loss moduli of tire components to tire energy losses. Rubber Chemistry and Technology 38(2), 400–414 (may 1965). https://doi.org/10.5254/1.3535661
6. Feldbrugge, J., Lehners, J.L., Turok, N.: Lorentzian quantum cosmology. Physical Review D 95(10) (may 2017). https://doi.org/10.1103/physrevd.95.103508
7. Finnveden, S.: Evaluation of modal density and group velocity by a finite element method. Journal of Sound and Vibration 273(1-2), 51–75 (may 2004). https://doi.org/10.1016/j.jsv.2003.04.004
8. Finnveden, S., Fraggstedt, M.: Waveguide finite elements for curved structures. Journal of Sound and Vibration 312(4-5), 644–671 (may 2008). https://doi.org/10.1016/j.jsv.2007.11.020
9. Kainradl, P., Kaufmann, G.: Heat generation in pneumatic tires. Rubber Chemistry and Technology 49(3), 823–861 (jul 1976). https://doi.org/10.5254/1.3534981
10. Kausel, E., Malischewsky, P., Barbosa, J.: Osculations of spectral lines in a layered medium. Wave Motion 56, 22–42 (jul 2015). https://doi.org/10.1016/j.wavemoti.2015.01.004
11. Kim, Y.J., Bolton, J.S.: Analysis of tire vibration by using a hybrid two-dimensional finite element based on composite shell theory. In: Proceedings of INTER-NOISE 2003. pp. 1344–1351. No. 294 (2003)
12. Korolkov, A., Shanin, A., Kniazeva, K.: Asymptotical study of two-layered discrete waveguide with a weak coupling. In: INTER-NOISE and NOISE-CON Congress and Conference Proceedings. vol. 261, pp. 5133–5144. Institute of Noise Control Engineering (2020)

13. Kung, L.E., Soedel, W., Yang, T.Y., Charek, L.T.: Natural frequencies and mode shapes of an automotive tire with interpretation and classification using 3-D computer graphics. Journal of Sound and Vibration 102(3), 329–346 (oct 1985). https://doi.org/10.1016/s0022-460x(85)80146-2

14. Loveday, P.W., Long, C.S., Ramatlo, D.A.: Mode repulsion of ultrasonic guided waves in rails. Ultrasonics 84, 341–349 (2018). https://doi.org/10.1016/j.ultras.2017.11.014

15. Neumann, J., Wigner, E.: ber das verhalten von eigenwerten bei adiabatischen prozessen. Phys. Zschr. 30, 467–470 (1929)

16. Nilsson, C.M.: Waveguide finite elements applied on a car tyre. Ph.D. thesis, Department of Aeronautical and Vehicle Engineering, Royal Institute of Technology (2004)

17. Press, F., Ewing, M., Tolstoy, I.: The Airy phase of shallow-focus submarine earthquakes. Bulletin of the Seismological Society of America 40(2), 111–148 (1950)

18. Randles, P.W.: Modal representation for the high-frequency response of elastic plates. Ph.D. thesis, Caltech, Pasadena, CA, 235 (1969)

19. Randles, P.W., Mlklowitz, J.: Modal representations for the high-frequency response of elastic plates. International Journal of Solids and Structures 7(8), 1031–1055 (aug 1971). https://doi.org/10.1016/0020-7683(71)90079-5

20. Sabiniarz, P., Kropp, W.: A waveguide finite element aided analysis of the wave field on a stationary tyre, not in contact with the ground. Journal of Sound and Vibration 329(15), 3041–3064 (jul 2010). https://doi.org/10.1016/j.jsv.2010.02.008

21. Shanin, A.V.: Precursor wave in a layered waveguide. The Journal of the Acoustical Society of America 141(1), 346–356 (jan 2017). https://doi.org/10.1121/1.4973958

22. Shanin, A.V., Knyazeva, K.S., Korolkov, A.I.: Riemann surface of dispersion diagram of a multilayer acoustical waveguide. Wave Motion 83, 148–172 (dec 2018). https://doi.org/10.1016/j.wavemoti.2018.09.010

23. Shanin, A.V., Korolkov, A.I., Kniazeva, K.S.: Integral representations of a pulsed signal in a waveguide. Acoustical Physics 68(4), 316–325 (aug 2022). https://doi.org/10.1134/s1063771022040108

24. Shanin, A.V., Korolkov, A.I., Kniazeva, K.S.: Saddle point method for transient processes in waveguides. Journal of Theoretical and Computational Acoustics 30(04) (mar 2022). https://doi.org/10.1142/s2591728521500183

25. Tolstoy, I.: Modes, rays, and travel times. Journal of Geophysical Research 64(7), 815–821 (jul 1959). https://doi.org/10.1029/jz064i007p00815

26. Waki, Y., Mace, B.R., Brennan, M.J.: Free and forced vibrations of a tyre using a wave/finite element approach. Journal of Sound and Vibration 323(3-5), 737–756 (jun 2009). https://doi.org/10.1016/j.jsv.2009.01.006

27. Wang, X. (ed.): Automotive tire noise and vibrations. Butterworth-Heinemann (2020)

28. Wheeler, R.L., Dorfi, H.R., Keum, B.B.: Vibration modes of radial tires: measurement, prediction, and categorization under different boundary and operating conditions. SAE Transactions 114, 2823–2837 (2005), http://www.jstor.org/stable/44725319